Destruction of Aqueous-Phase Carbon Tetrachloride in an Electrochemical Reactor with a Porous Cathode

ARTICLE *in* INDUSTRIAL & ENGINEERING CHEMISTRY RESEARCH · JANUARY 2004

Impact Factor: 2.59 · DOI: 10.1021/ie030591c

Destruction of Aqueous-Phase Carbon Tetrachloride in an Electrochemical Reactor with a Porous Cathode

Jiahan He,[†] A. Eduardo Sáez,*[,†] Wendell P. Ela,[†] Eric A. Betterton,[‡] and Robert G. Arnold[†]

Department of Chemical and Environmental Engineering and Department of Atmospheric Sciences, University of Arizona, Tucson, Arizona 85721

In this work we investigate the use of a continuous-flow, laboratory-scale electrochemical reactor for the destruction of aqueous-phase carbon tetrachloride (CT). The reactor consists of a porous copper foam cathode and a carbon-cloth anode section located downstream from the cathode. Experimental results show that appreciable conversions of CT can be obtained in the reactor, as long as the electrical conductivity of the liquid exceeds 1 S/m. At lower conductivities, most of the cathode exhibits low reactivity for CT-destruction due to relatively low charge transfer overpotentials. A mathematical model was formulated to predict reactor performance. The model takes into account the CT-reduction reaction and the hydrogen evolution reaction on the cathode surface as well as mass transfer limitations. Using the equilibrium potential for CT reduction as the only adjustable parameter, the model adequately represents experimental data for highly conductive solutions.

Introduction

Low-molecular-weight chlorinated compounds are among the most pervasive contaminants in soil and groundwater. Widespread use of chlorinated methanes, ethanes, and ethenes, primarily as industrial solvents, and inattention to proper disposal methods produced the current situation. These compounds are prominent pollutants at National Priority List sites. Carbon tetrachloride (CT), trichloroethylene, and perchloroethylene have been assigned drinking water maximum contaminant levels in the range 1−5 μg/L because of their status as suspected carcinogens.

A number of physical and biochemical technologies have been applied to remediate groundwater contaminated with chlorinated solvents with limited success. Representative physical strategies include pump-and-treat methods and air sparging. Experience has shown that these processes are much slower and more costly than originally expected due to contaminant rebound (pump-and-treat) and channeling/sphere-of-influence considerations (air sparging). When these strategies successfully remove contaminants from groundwater, additional treatment steps are required for contaminant destruction or final disposal. When advanced oxidation technologies are employed, their success depends on adequate dispersal of strong oxidants such as ozone, hydrogen peroxide, or permanganate in zones of contamination. Incineration of gas- or liquid-phase halohydrocarbons can produce dioxins and furans, and such processes are sometimes discouraged. Biological transformations can depend on the encouragement and sustenance of capable bacterial types, and in some cases biochemical transformation intermediates are more toxic than precursor compounds. Intrinsic bioremediation methods are usually selected when more aggressive remedies prove to be ineffective or unacceptably expensive.

Because of the electronegative character of halogen substituents, heavily chlorinated compounds are thermodynamically disposed to act as electron acceptors in redox reactions.[1,2] Zerovalent metals and reduced, metal-containing enzymes and coenzymes can serve as effective reductants for dehalogenation reactions.[3−9] Reductive dechlorination using zerovalent metals has received considerable attention as an in situ remediation tool for contaminated groundwater or as a reactive barrier to groundwater transport. Potential disadvantages of reactive barriers containing Fe(0) include the release of soluble metal, formation of insoluble oxide coatings on elemental metal surfaces, and hydrogen generation. Halohydrocarbons can also be reduced electrochemically without releasing metal ions or passivating electrode surfaces with metal oxides. Through judicious selection of cathode materials and electrical potential, reduction of halogenated targets can yield alkanes or alkenes that are environmentally benign. Copper and nickel electrodes are particularly useful in this regard.[10]

The kinetics of electrochemical reduction can be governed by mass transport and/or rate of charge transfer at the electrode surface.[11] Charge-transfer rates are a function of electrode material as well as overpotential. Various materials have been studied for electrochemical dechlorination including a number of elemental metals,[10−14] graphite,[13] glassy carbon,[15] conductive ceramics,[16] and composite materials.[17]

Here we describe efforts to develop, test, and model a continuous-flow, one-dimensional electrochemical reactor for the destruction of halogenated hydrocarbons in water. Carbon tetrachloride was selected as the target compound for related experiments. Our objective is to establish the conditions necessary for rapid, efficient conversion of CT to dechlorinated products and to characterize transformation kinetics in terms of parameters that are within the control of process designers.

Modeling

Process Description. The continuous-flow reactor and experimental configuration used in this work are

* To whom correspondence should be addressed. Phone: (520) 621-5369. Fax: (520) 621-6048. E-mail: esaez@engr.arizona.edu.
[†] Department of Chemical and Environmental Engineering.
[‡] Department of Atmospheric Sciences.

10.1021/ie030591c CCC: $27.50
Published on Web 01/14/2004

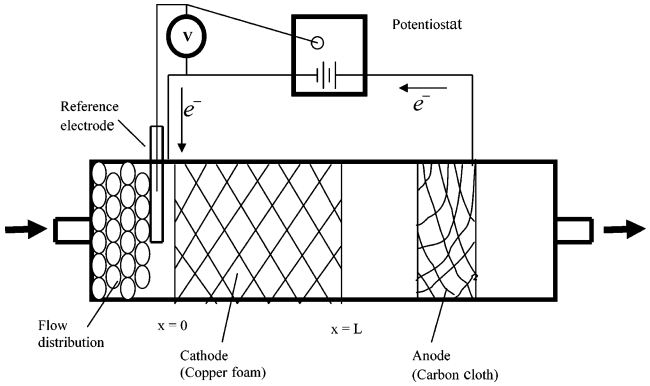

Figure 1. Schematic of the electrochemical reactor. The CT aqueous solution first flows through a 3-cm deep flow distribution section packed with sand. It then enters the reactor's cathode section, which consists of a porous copper foam. The cathode section has a length (L) of 4 cm. The anode (carbon cloth) is located 2 cm downstream from the end of the cathode. A potentiostat was used to control the applied potential on the cathode. An Ag/AgCl reference electrode was placed 0.5 cm upstream from the cathode.

shown in Figure 1. There are three reactor sections: a flow distribution section packed with sand, a cathode section consisting of a porous copper foam, and a carbon-cloth anode section that is positioned downstream from the cathode. The CT-laden solution flows through the flow distribution section before entering the copper foam. The cathode potential was fixed at levels from −0.1 to −0.8 V vs SHE (standard hydrogen electrode) using a potentiostat. Reactions at the cathode include the conversion of CT to methane

$$CCl_4 + 4H^+ + 8e^- \rightarrow CH_4 + 4Cl^- \tag{1}$$

and hydrogen evolution

$$H_2O + e^- \rightarrow \frac{1}{2}H_2 + OH^- \tag{2}$$

Water reacts to achieve equilibrium with its ion products:

$$H_2O \leftrightarrow H^+ + OH^- \tag{3}$$

Thus, the pH of the solution will increase as a result of reaction within the copper foam.

The primary reaction at the anode is the oxidation of water to oxygen:

$$H_2O \rightarrow \frac{1}{2}O_2 + 2H^+ + 2e^- \tag{4}$$

Theoretical Equations. The configuration of the cathode and the uniformity of conditions at its upstream end allow us to assume that the concentrations of reactants and products are uniform over the cross section of the reactor. Furthermore, longitudinal dispersion is assumed to be negligible under the experimental conditions employed: the presence of the porous copper foam ensures a flat velocity profile on the cross section of the cathode without inducing appreciable hydrodynamic dispersion in the direction of flow due to the relatively high porosity of the medium. Therefore, plug flow is assumed throughout the balances presented below. A mole balance on CT at steady-state yields

$$U_{av}\frac{dC_b}{dx} = -aJ_m \tag{5}$$

where U_{av} is the superficial liquid velocity (m/s), C_b is the bulk concentration of CT (mol/m^3), a is the surface area of the copper foam per unit reactor volume (1/m), and J_m is the mass transfer flux from the liquid phase to the surface of the electrode (mol/m^2 s). Mole balances for proton and hydroxide ion yield

$$U_{av}\frac{dC_H}{dx} = R_H - R_W \tag{6}$$

and

$$U_{av}\frac{dC_{OH}}{dx} = -R_W \tag{7}$$

where C_{OH} and C_H are the concentrations of hydroxide ion and hydrogen ion (mol/m^3), respectively, R_H is the rate of the hydrogen evolution reaction (HER) (eq 2), and R_W is the net rate of the water dissociation reaction (eq 3) (mol/m^3 s). Combining eqs 6 and 7 with the ion product for water ($K_W = C_H C_{OH}$), and solving for the gradient of hydrogen concentration yields

$$\frac{dC_H}{dx} = -\frac{R_H}{U_{av}\left(1 + \frac{K_W}{C_H^{\,2}}\right)} \tag{8}$$

Here we have assumed that the water dissociation reaction is instantaneous, so that the concentrations of H^+ and OH^- satisfy the equilibrium ion product for water at all times.

The current generated in the cathode is the sum of the currents required by reactions 1 and 2:

$$i_t = i_{CT} + i_H \tag{9}$$

where i_t is the total current density (total accumulated current per unit cross-sectional area of reactor, A/m^2), and i_{CT} and i_H are the accumulated current densities due to reactions 1 and 2, respectively. Thus, eqs 5, 8, and 9 describe changes in concentration and current within a section of the cathode. In an electrochemical system, the magnitude of these changes is related to the energy added to the system as electrical potential. Governing relationships are developed below.

The rate of disappearance of CT is limited by the rate of charge transfer at the electrode surface, the mass transfer rate to the electrode, or a combination of the two. When the reaction of CT is controlled by charge transfer kinetics (usually when the magnitude of the cathode overpotential is relatively small), the CT concentration at the electrode surface is similar to the bulk concentration of CT. On the other hand, if CT transformation is dominated by the rate of mass transfer to the electrode, the CT concentration at the cathode surface would be essentially zero. Between those two limiting cases, the rate of disappearance is a function of both charge transfer and transport rates.

The flux of CT from bulk liquid phase to the surface of the electrode is given by

$$J_m = k_L(C_b - C_s) \tag{10}$$

where the mass transfer coefficient, k_L (m/s), is assumed to be constant throughout the porous electrode, and C_s is the concentration of CT at the electrode surface (mol/m^3). The mass transfer coefficient was estimated from the following empirical correlation[18]

$$k_L = 0.52\frac{D}{d}\mathrm{Re}^{0.5}\mathrm{Sc}^{0.37} \tag{11}$$

where D is the diffusivity of CT in water (m^2/s), d is the diameter (m) of the metal fibers that comprise the copper foam,[19] the Reynolds number is defined as $\mathrm{Re} = U_{av}d/\epsilon\nu$, and the Schmidt number is $\mathrm{Sc} = \nu/D$, where ϵ is the porosity of the copper foam and ν is the kinematic viscosity of the solution.

The rate of reaction is given by

$$J_r = k_c C_s \exp\left(\frac{-Z_0 \alpha F \eta}{RT}\right) \tag{12}$$

where J_r represents the reaction rate (moles of CT consumed per unit time and electrode surface area), and k_c is the surface-area-normalized reaction rate constant (m/s). In the exponential term, Z_0 is the number of electrons transferred in the rate-limiting reaction step (see below), and α is the transfer coefficient that reflects the efficiency with which electrical energy supplied to the cathode is used to overcome the reaction activation energy. The value of α is 0.28 for the electrochemical degradation of CT on copper.[10] In eq 12, η is the charge-transfer overpotential (V), F is Faraday's constant (coulomb/mol), R is the gas constant (J/K·mol), and T is the absolute temperature (K).

Under steady conditions, the mass flux is equal to the reaction rate. Hence, eqs 10 and 12 can be combined to solve for C_s, which yields

$$C_s = \frac{k_L C_b}{k_L + k_c \exp\left(\frac{-Z_0 \alpha F \eta}{RT}\right)} \tag{13}$$

The charge-transfer overpotential is defined by

$$\eta = E - E_{eq} - \eta_c - \phi_s \tag{14}$$

where E is the potential applied to the cathode, which is assumed to be uniform throughout the porous electrode since the effective conductivity of the metal phase is much greater than that of the solution; E_{eq} is the equilibrium potential of the rate-limiting reaction step; η_c is the concentration overpotential and ϕ_s is the solution potential. Reaction 1 proceeds via a mechanism in which the rate-limiting step is the formation of tricholoromethyl radical ($\cdot CCl_3$),[20] so that $Z_0 = 1$. Because the trichloromethyl radical concentration is not readily measured or predicted at the electrode surface to confirm that its formation is the rate-limiting step, the equilibrium potential, E_{eq}, is used as an adjustable parameter in this work.

The concentration overpotential, η_c, is the change in overpotential due to reactant concentration differences between the bulk solution and electrode surface. A depletion of reactive species occurs in the electrolyte solution adjacent to the electrode. The concentration overpotential is small when the concentration of the target compound at the electrode surface is close to that of the bulk solution, i.e., when the reaction rate is determined primarily by charge transfer kinetics. Thus, the concentration overpotential should be minimal at relatively low (less negative) cathode potentials. The concentration overpotential is calculated from[21]

$$\eta_c = -\frac{RT}{Z_0 F}\ln\left(\frac{C_b}{C_s}\right) \tag{15}$$

The gradient of the solution potential is related to the total current density by

$$i_t = -\kappa \frac{d\phi_s}{dx} \tag{16}$$

where κ is the effective conductivity of the solution in the cathode compartment (S/m), calculated from[21]

$$\kappa = \kappa_0 \epsilon^{1.5} \tag{17}$$

where κ_0 is the conductivity of the solution and ϵ is the porosity of the cathode.

The relationship between the hydrogen production rate and hydrogen overpotential (η_H) is given by Tafel's equation:

$$\eta_H = a_T + b_T \log j_H \tag{18}$$

where a_T and b_T are constants, and j_H is the hydrogen point current density based on the electrode surface area, given by

$$j_H = \frac{1}{a}\frac{di_H}{dx} \tag{19}$$

The hydrogen overpotential is given by

$$\eta_H = E - E_{H,eq} - \phi_s \tag{20}$$

in which the equilibrium potential for hydrogen evolution is given by

$$E_{H,eq} = E_{H,eq}{}^0 - \frac{RT}{F}\ln P_{H2}{}^{1/2} C_{OH} \tag{21}$$

where C_{OH} is the concentration of hydroxide ion (mol/L in this equation), $E_{H,eq}{}^0$ is the equilibrium potential under standard conditions

$$\left(E_{H,eq}{}^0 = -0.82\ \mathrm{V} = -\frac{RT}{F}\ln P_{H2}{}^{1/2}/K_W\right)$$

and P_{H2} is the partial pressure of hydrogen at the surface of electrode, here assumed to be 1 atm. Combining eqs 18−21 leads to

$$E - E_{H,eq}{}^0 + \frac{RT}{F}\ln C_{OH} - \phi_s = a_T + b_T \log j_H \tag{22}$$

Problem Formulation. The governing equation for CT concentration is obtained by substituting the mass transfer flux relationship (eq 10) into the mass balance (eq 5) to obtain

$$\frac{dC_b}{dx} = -\frac{ak_L}{U_{av}}(C_b - C_s) \tag{23}$$

Recall that C_s is represented in terms of the bulk concentration and local overpotential (eq 13).

Table 1. Summary of Simultaneous Equations That Integrate the Model

dependent variable	governing equation
C_b, bulk CT concentration	23, boundary condition 28
C_s, CT concentration on cathode surface	13
C_H, bulk H^+ concentration	25, boundary condition 28
C_{OH}, bulk OH^- concentration	$C_{OH} = K_W/C_H$
ϕ_s, solution potential	26, boundary condition 30
j_H, current density associated with H_2 generation, based on cathode surface area	22
i_H, cumulative current density associated with H_2 generation, based on reactor's cross-sectional area	19, boundary condition 29
i_{CT}, cumulative current density associated with CT reduction, based on reactor's cross-sectional area	31
η, overpotential	14
η_c, concentration overpotential	15

The governing equation for the hydrogen ion concentration is derived from eq 8, noting that

$$R_H = \frac{aj_H}{F} \tag{24}$$

which yields

$$\frac{dC_H}{dx} = -\frac{aj_H}{U_{av}F\left(1 + \frac{K_W}{C_H^2}\right)} \tag{25}$$

The solution potential is governed by eq 16 which, using eq 9, can be rewritten as

$$\frac{d\phi_s}{dx} = -\frac{(i_H + i_{CT})}{\kappa} \tag{26}$$

The gradient of the current density due to CT conversion is derived from the following charge balance

$$\frac{di_{CT}}{dx} = -U_{av}ZF\frac{dC_b}{dx} \tag{27}$$

where, for CT conversion to methane, $Z = 8$ (eq 1).

The previous system of differential equations is subject to the following boundary conditions: first, inlet concentrations are prescribed

$$C_b = C_{bin},\ x = 0$$
$$C_H = C_{Hin},\ x = 0 \tag{28}$$

At the entrance to the cathode section of the reactor, the current density associated with each reaction is zero

$$i_t = i_{CT} = i_H = 0,\ x = 0 \tag{29}$$

and the solution potential is assigned a value of zero at the downstream end of the cathode[21,22]

$$\phi_s = 0,\ x = L \tag{30}$$

This boundary condition for solution potential is valid only when the solution conductivity is relatively high (see Results and Discussion section).

Using boundary conditions 28 and 29, eq 27 can be integrated to find

$$i_{CT} = -U_{av}ZF(C_b - C_{bin}) \tag{31}$$

Table 1 summarizes the formulation of the model. It consists of four first-order ordinary differential equations plus 6 nonlinear algebraic equations that must be solved simultaneously.

Solution Procedure. The four differential equations (Table 1) were discretized using a first-order forward difference approximation (Euler's method), with a uniform interval size throughout the solution domain ($0 < x < L$). Typically, 400 intervals were enough to find a converged solution for which further refinement did not change calculated values appreciably.

The boundary conditions for concentrations and current densities (eqs 28 and 29) are imposed at the upstream end of the cathode. However, because the boundary condition for the potential is specified at the downstream end (eq 30), the problem becomes a boundary-value problem. To solve it, we used an iterative technique that starts by assuming a value for ϕ_s at $x = 0$ (ϕ_{s0}), thereby transforming the discretized problem into an initial value problem. The most common iteration technique in this type of situation would be to calculate the value of ϕ_s at $x = L$, and iterate (varying ϕ_{s0}) until the desired boundary condition (eq 30) is achieved. However, we have found that it is more efficient in terms of number of iterations to proceed with the solution (using Euler's method) by stepping in the x direction until the condition $\phi_s = 0$ is achieved. This happens, in general, at $x = L'$. At this point, Euler's method is stopped and the value of ϕ_{s0} is modified according to

$$\phi_{s0n} = \phi_{s0} + \frac{1}{10^3}\log\left(\frac{L'}{L}\right) \tag{32}$$

This adjustment function was selected after a linear adjustment strategy failed to yield converged solutions. The stepwise calculation is repeated until $|L' - L|/L \leq 10^{-3}$. This procedure led to a converged solution in 500−1500 iterations.

During the solution procedure, C_b, C_H, ϕ_s, and i_H are determined for a particular grid point in x from values of the dependent variable in the previous point (Euler's method). Once these values are calculated, the remaining algebraic equations (eqs 13−15, 22, and 31, Table 1) constitute a nonlinear set of equations that was solved by a direct iteration method with relaxation.

Material and Methods

Experimental Setup. Figure 1 illustrates the experimental setup used in the study. The reactor was manufactured from a Plexiglas tube with an inner diameter of $1^1/_4$ in. It was operated vertically in up-flow mode to facilitate the release of hydrogen bubbles. Carbon-tetrachloride-laden water entered the reactor from the base. A 3-cm sand bed provided a flow

distribution zone. A Ag/AgCl reference electrode (Thermo Orion, Beverly, MA) was inserted 0.5 cm above the surface of the sand bed and 0.5 cm below the entrance to the porous copper cathode. The copper foam cathode material (Electrosynthesis, Lancaster, NY) had a porosity of 95% and a specific surface area of 1100 m^2/m^3 (manufacturer's data). It was cut into $1^1/_4$-in.-diameter disks with thickness of about 0.5 cm. Several disks were stacked together to produce the desired cathode length. The potential drop across the cathode was negligible in all the experiments performed.

The disks were soaked in 2% Micro-90 cleaning solution (Cole-Parmer, Vernon Hills, IL) and placed on a shaking bed for at least 3 days prior to each experiment. The cleaning solution was changed every day. Before use, the disks were rinsed using high purity water (Milli-Q water systems, Millipore Company, Bedford, MA). Carbon cloth (Electrosynthesis) was used as the anode. The cathode potential was fixed using a potentiostatic controller (Electrosynthesis) that was connected to a DC power supply (Harrison Laboratories, Parker, CO).

Chemicals and Solutions. All chemicals were used as purchased. The electrolyte solution was made by adding potassium sulfate (99+%, EM Science, Gibbstown, NJ) to high purity water to produce target solution conductivities.

The solutions for measurement of hydrogen-evolution reaction rates were prepared by adding buffers to the original electrolyte solution. The pH 7.2 buffer was obtained by dissolving monobasic potassium phosphate and dibasic potassium phosphate at a molar ratio of 1:1. The pH 10.3 buffer contained equimolar concentrations of potassium carbonate and potassium bicarbonate, and the buffer solution at pH 12.3 was obtained with equimolar concentrations of dibasic potassium phosphate and tribasic potassium phosphate. The strengths of all three buffer solutions were 2 μM. The buffer solutions were purged with argon for 3 h to eliminate dissolved oxygen before use.

Target influent CT concentrations were obtained by adding pure CT (99.5+%, Aldrich Chemical Co., Milwaukee, MI) to the argon-purged electrolyte solutions. Solutions were then mixed for 24 h using a magnetic stirring bar to guarantee complete dissolution. No pH buffers were used when the reactor was employed to destroy CT. The influent CT concentration was 12.5 μM. Representative experiments were run to confirm that the fractional removal of CT in the reactor was independent of influent concentration in the range 6−20 μM.

Experimental Procedure. All experiments were conducted at room temperature (approximately 25 °C). The cathode potential was set after the reactor was completely filled with the influent solution. Samples were taken after steady conditions were achieved (usually 30 min after the cathode potential was set). Steady-state conditions were verified when measured exit concentrations did not change with time. The cathode potential was monitored using a Fluke 73 III Multimeter (Fluke Corp., Everett, WA) that measured the potential difference between the cathode and reference electrode. The current was monitored using a model 197 auto-ranging microvolt DMM (Keithley Instruments, Inc., Cleveland, OH). The flow rate was measured volumetrically.

Sampling and Analysis. Water samples (50 μL) were withdrawn from the reactor through sampling ports located at $x = 0$, 1, 2, 3, and 4 cm from the cathode inlet using a glass syringe. Samples were immediately transferred to sealed vials containing 1 mL of heptane (Burdick & Jackson, Muskegon, MI). Three samples were taken for each point and their CT concentration was averaged.

Heptane extracts were analyzed for CT on a HP 5890 gas chromatograph (Hewlett-Packard, St. Paul, MN). The GC was equipped with a capillary column (J & W Scientific, column DB-624) and electron capture detector. The gas flowrate was 26 mL/min. The temperatures of oven, detector, and inlet were set at 40, 275, and 150 °C, respectively.

Product Identification. Liu et al.[10] observed that the electrochemical reduction of CT on iron, nickel, and copper electrodes in a batch system produced a temporary accumulation of metastable reduction intermediates, including chloroform. Chloroform was subsequently converted to methane and CH_2Cl_2. Copper and nickel provided both favorable reduction kinetics and relatively high CH_4/CH_2Cl_2 ratios. In this study, chlorinated intermediates were always below GC detection limits; methane was assumed to be the primary conversion product.

Results and Discussion

The hydrogen evolution reaction was first studied in the absence of CT in order to establish the Tafel constants for our experimental system. Experiments with CT followed. The results were used to calibrate the mathematical model. Model simulations were performed to investigate the sensitivity of reactor performance to operational variables and to determine whether the reactor was charge-transfer or mass-transfer limited.

Hydrogen Evolution Reaction. Aqueous-phase cathode processes often proceed parallel to the reduction of water, limiting the overall current efficiency, defined in terms of the fraction of reducing equivalents that are used to convert target to product. The relation between the current and overpotential for hydrogen evolution is described by Tafel's equation. The current−overpotential relation depends on many factors, among which electrode material and electrode surface conditions are of particular importance. The coefficient b_T (eq 18) is relatively constant for different electrode materials and different surface conditions, with the exception of metals that strongly adsorb hydrogen, e.g., platinum and palladium. However, values for the coefficient a_T vary considerably even for a single electrode material. This is generally attributed to variation in the electrode surface condition and solution purity.[21]

To evaluate Tafel coefficients for our experimental conditions, a single 0.5-cm-thick copper foam disk was used as cathode, and solutions at several fixed pHs were passed through the reactor. Three different solution pHs were studied: phosphate-buffered solutions with pHs of 7.2 and 12.3, and a carbonate-buffered solution at pH 10.3. Current densities were obtained by dividing the observed currents by the total electrode surface area. The overpotential was calculated using eq 19, assuming that the change in solution potential was negligible across the 0.5-cm electrode. Data on the relation between current density and overpotential for the reduction of water on the copper cathode are presented in Figure 2. The Tafel coefficients obtained in this manner ($a_T = -0.216$, $b_T = -0.129$) are comparable to those reported previously.[23]

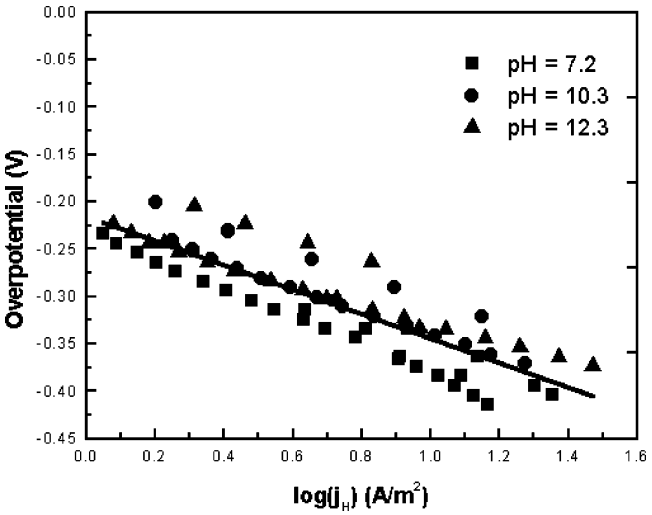

Figure 2. Relation between overpotential and current density for the hydrogen evolution reaction. The solution conductivity is 2.3 S/m. The solid line is a fit of all the data using Tafel's equation (eq 18) with $a_T = -0.216$ and $b_T = -0.129$.

The results in Figure 2 correspond to several experiments. Results from a given experiment do not show great scatter and follow a well-defined trend. However, results from different experiments and the same conditions show some noticeable differences. We believe that this is a result of slight variations in cathode surface conditions. Inter-experiment variations in a series of identical CT-free experiments were similar in magnitude to variations produced by changing pH from 7.2 to 12.3. Thus, it was concluded that pH has a negligible influence on the Tafel coefficients within the limitations of the experiment. The regression line in Figure 2, based on results from all CT-free experiments, was used to relate hydrogen generation to cathode potential in all subsequent model simulations.

Destruction of Carbon Tetrachloride. Carbon tetrachloride conversion experiments were conducted using flow rate, cathode potential, and solution conductivity as independent variables. Simulations were performed for the same set of experimental conditions. The effect of cathode potential on CT removal is illustrated in Figure 3(a). The total removal of CT in the reactor increased from 36% to 71% when the cathode potential was decreased from −0.1 V (reported potentials are vs SHE unless otherwise stated) to −0.4 V. Further decrease in cathode potential from −0.4 to −0.8 V increased the removal only from 71% to 83%. No conversion was observed when the cathode potential was 0 V. Model calibration was carried out using a single fitting parameter, the equilibrium potential, to optimize agreement between prediction and observation; the fitted value was $E_{eq} = 0.5$ V. All subsequent simulations were carried out using this value. The standard equilibrium potential for the rate-limiting reaction step (charge transfer to CT to produce trichloromethyl radical) has been estimated at −3.1 V.[20] The difference between the fitted value and standard potential can be reconciled only if the trichloromethyl radical is exceptionally reactive.

The effect of superficial electrolyte velocity on observed CT removal is shown in Figure 3(b). When the liquid velocity was increased from 0.022 cm/s to 0.047 cm/s, the rate of CT conversion in terms of concentration decay per unit residence time increased slightly due to enhanced mass transfer, but the overall removal decreased from 83% to 60% because of the abbreviated hydrodynamic retention time. Again, simulations were

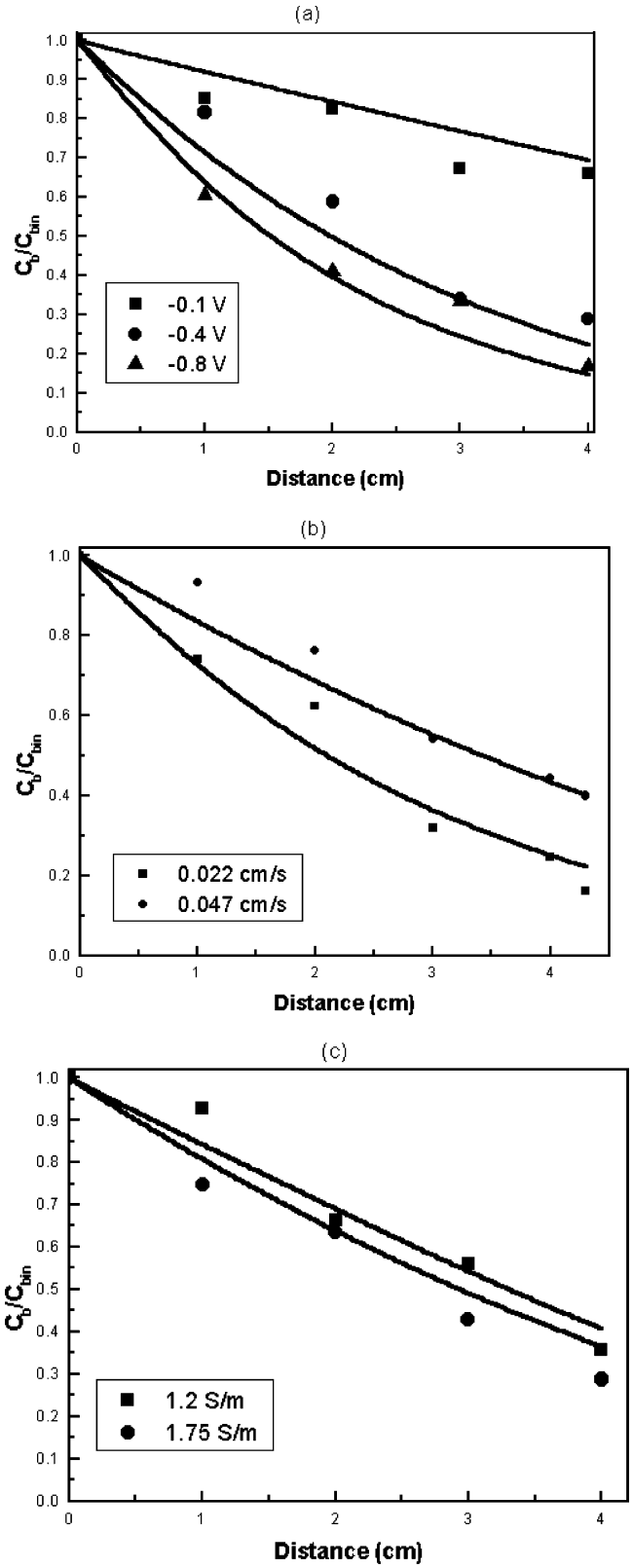

Figure 3. Normalized CT concentration profiles in the reactor for various operating conditions. The symbols are experimental data and the solid lines are model predictions. (a) The liquid superficial velocity is 0.014 cm/s, and the conductivity of the solution is 2.7 S/m. The legend shows applied cathode potential. (b) The applied cathode potential is −0.6 V, and the solution conductivity is 2.7 S/m. The legend shows liquid superficial velocity. (c) The liquid velocity is 0.032 cm/s, the cathode potential is −0.55 V. The legend shows solution conductivity.

performed using an equilibrium potential of 0.5 V, and reasonable agreement between experiments and predictions was obtained.

When the solution conductivity was increased from 1.20 S/m to 1.75 S/m, CT removal increased from 64% to 73% (Figure 3c). These results show that reactor performance and model simulations are relatively insensitive to solution conductivity in this range.

The CT destruction reaction has a net effect of increasing OH^- concentration (and thus pH) along the reactor. Typically, the pH increased from approximately 7 (inlet solution) to between 10 and 11 at the end of the cathode.

Model Predictions. Agreement between the results of experiments and simulations indicates that the model can be used to predict CT transformation in the reactor. The calibrated model was therefore applied to a series of hypothetical cases to better understand the effects of operational variables on reactor performance. Simulations also allowed us to distinguish between the contributions of HER and CT reduction to overall reactor current.

The predicted effect of cathode potential on reactor CT profiles is illustrated in Figure 4(a). In the range $-0.1\ \text{V} > E_c > -0.6\ \text{V}$, total CT removal increased from 37% to 87%. Applied potentials below −0.6 V are predicted to have little effect on CT removal. Reduction of cathode potential below this value causes accelerated hydrogen production, with consequent increases in the magnitude of solution potential. The contribution of hydrogen reduction to the local current density in the cathode section is shown in the Figure 4(b) profiles. Note the substantial increase of this contribution at potentials from −0.4 to −0.8 V. Current densities for CT reduction (not shown) are in the range $0-7\ \text{A/m}^2$ and become insensitive to applied potential below −0.6 V (Figure 4a). The hydrogen evolution reaction continues to accelerate throughout the range of potentials simulated because the reduction of water is not subject to the same mass transfer limitation as CT reduction at the most negative voltages used in the simulations.

The lack of sensitivity of CT concentration profiles to applied potential below −0.6 V is attributable, at least in part, to development of a substantial solution potential, or the energy consumed to drive charge through the solution to complete the electrolytic circuit. Predicted solution potentials are presented as a function of position in the cathode section and the cathode potential in Figure 4(c). Solution potential is predicted to grow rapidly with distance in the cathode when E_c is −0.4 V or below. Furthermore, the predicted solution potential is most negative at the upstream end of the cathode and increases along the length of the electrode. In the last centimeter of the cathode, the gradient in solution potential is most severe, as expected from current density considerations (eq 24). It is apparent that at the most negative potentials simulated, much of the cathode is operated at low efficiency due to the effect of solution potential on the cathode overpotential (eq 14).

The relation between solution potential at the influent end of cathode and cathode potential is illustrated in Figure 5. Clearly, when cathode potential is more negative than −0.6 V, the local solution potential decreases almost linearly with the change in cathode potential (slope ≅ 0.9), suggesting that virtually all of the additional energy applied to the cathode is consumed by charge transport in the liquid phase. Because most of this charge is derived from the reduction of water (Figure 4c), cathode potentials lower than −0.6 V do little to promote CT reduction.

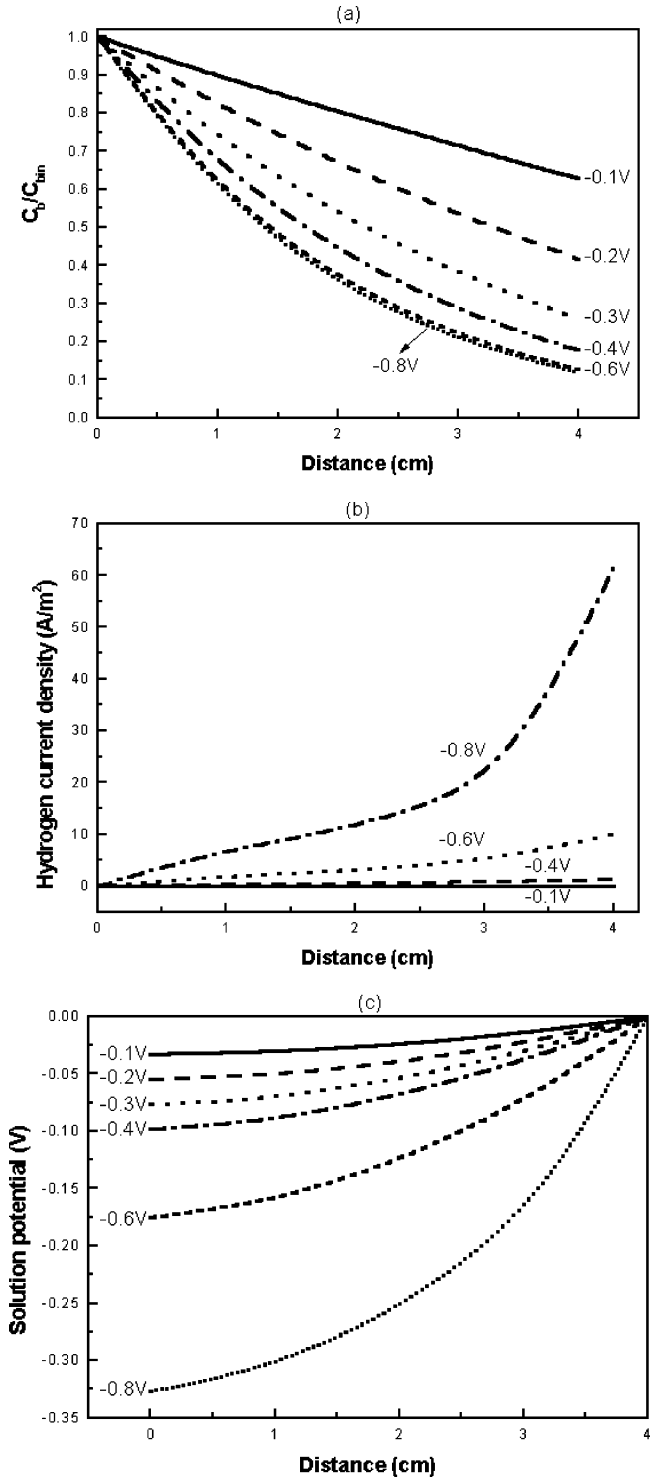

Figure 4. Model predictions on the effect of cathode potential on: (a) CT concentration profiles, (b) hydrogen current density profiles, and (c) solution potential profiles. In all cases, the liquid superficial velocity is 0.01 cm/s, and the solution conductivity is 2 S/m.

The effects of solution conductivity on overall reactor performance are illustrated in Figure 6. Through-reactor CT removal increases monotonically with conductivity in the range $0.05\ \text{S/m} < \kappa_0 < 4.0\ \text{S/m}$ (Figure 6a, b). A conductivity of 0.05 S/m corresponds to a 300 mg/L concentration of K_2SO_4. Water with less than 1000 mg/L

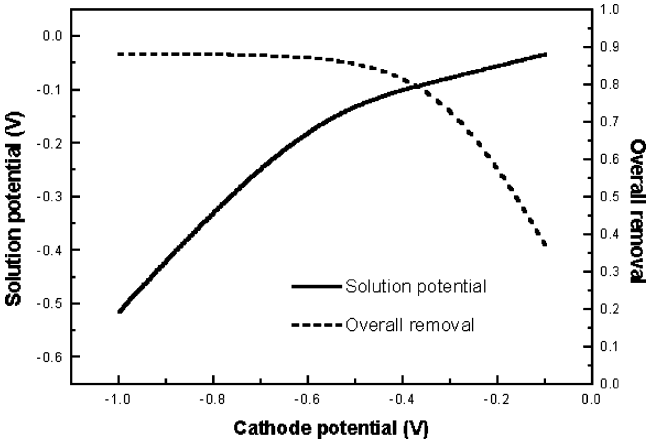

Figure 5. Predicted change of overall CT removal fraction and solution potential at the entrance of cathode with applied cathode potential. The liquid superficial velocity is 0.01 cm/s, and the solution conductivity is 2 S/m. For low applied cathode potentials, the relation between solution and cathode potentials is linear.

total dissolved solids is classified as freshwater.[23] At the lowest conductivities simulated, much of the cathode is inactive in terms of CT consumption, and CT removal occurs primarily at the downstream end of the cathode. At higher conductivities, the entire cathode contributes to CT destruction (Figure 6a). Again, the relationship between solution potential and conductivity is central to electrode behavior. Overall CT removal efficiency is predicted to drop off rapidly when $\kappa_0 < 2$ S/m (Figure 6b). This effect is particularly marked at conductivities below about 0.5 S/m. These calculations show that contaminated freshwaters will be difficult to remediate in the electrolytic reactor configured as shown in Figure 1. That is, conductivities on the order of 0.05−0.10 S/m lead to solution potentials that severely limit the overpotential for charge-transfer reactions in the upstream sections of the cathode (Figure 6c).

The model was used to explore the effect of hydrodynamic residence time, defined as HRT $= L/U_{av}$, on reactor performance. The HRT can be adjusted by changing either the liquid velocity (increasing the reactor diameter for a fixed flow rate of liquid) or the cathode length. Both approaches were simulated in this work. Figures 7(a) and (b) show how HRT affects CT removal and solution potential at the entrance of the cathode, for two different solution conductivities. For the high-solution-conductivity case ($\kappa_0 = 2$ S/m), CT removal was essentially independent of the method chosen to increase HRT, up to HRT = 15 min (Figure 7a). For higher residence times, CT removal becomes insensitive to cathode length (constant liquid velocity) but it continues to increase with decreasing liquid velocity at constant cathode length. At the lower conductivity ($\kappa_0 = 0.05$ S/m), increasing HRT by increasing the cathode length has little or no effect on reactor efficiency for HRT ≥ 3 min. This again indicates that increasing reactor length to promote contaminant removal in a relatively low ionic strength solution is of little value. Corresponding solution potentials predicted at the entrance of the porous cathode are shown in Figure 7(b). It is apparent that, irrespective of solution conductivity, increasing HRT by decreasing liquid velocity (i.e., increasing reactor cross-section) is more efficient than increasing reactor length, primarily as a consequence of solution potential. For the same HRT values, the larger, narrower reactor configuration increases the solution potential at the reactor inlet (and presumably

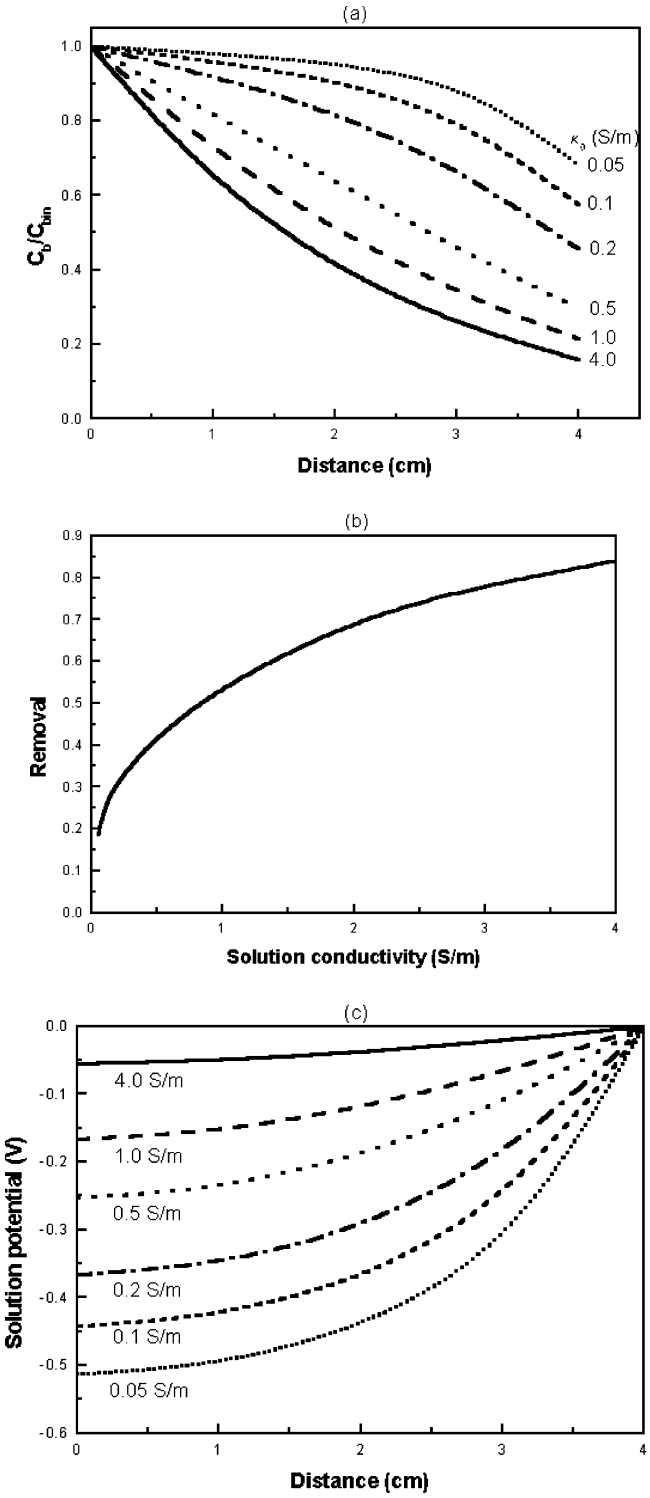

Figure 6. Effect of solution conductivity on predicted (a) CT concentration profiles, (b) overall removal fraction ($1 - C_b/C_{bin}$), and (c) solution potential profiles. The applied cathode potential is −0.4 V, the liquid superficial velocity is 0.01 cm/s.

over much of the upstream reactor section) as charge must be transferred over greater distances to complete the electrolytic circuit.

Sensitivity Analysis. Given the uncertainties associated with the experimental determination of the coefficients for Tafel's equation (eq 18 and Figure 2), and in order to evaluate the effect of water reduction on the removal of CT, we examined the sensitivity of CT concentration profiles to changes in the current density due to hydrogen evolution. For this purpose, we

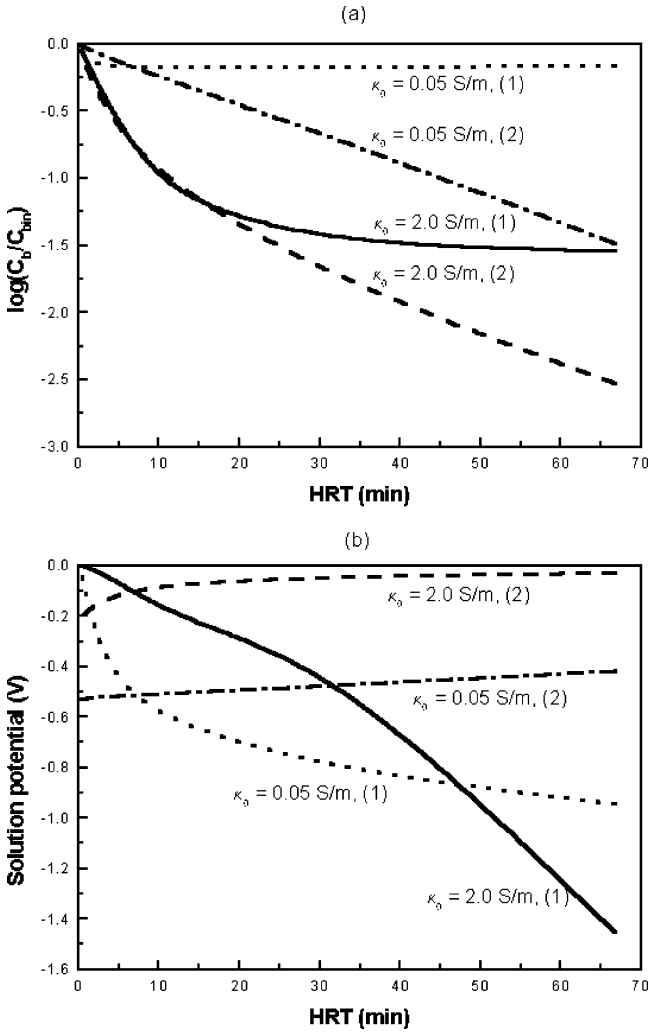

Figure 7. Effect of hydrodynamic residence time (HRT) on (a) CT removal, and (b) solution potential at the entrance of the cathode, for different solution conductivities. For the results labeled as (1), HRT was changed by changing the length of the cathode for a fixed liquid superficial velocity of 0.01 cm/s. For the results labeled as (2), HRT was changed by changing the liquid velocity for a fixed length of cathode of 4 cm. All results correspond to an applied cathode potential of −0.4 V.

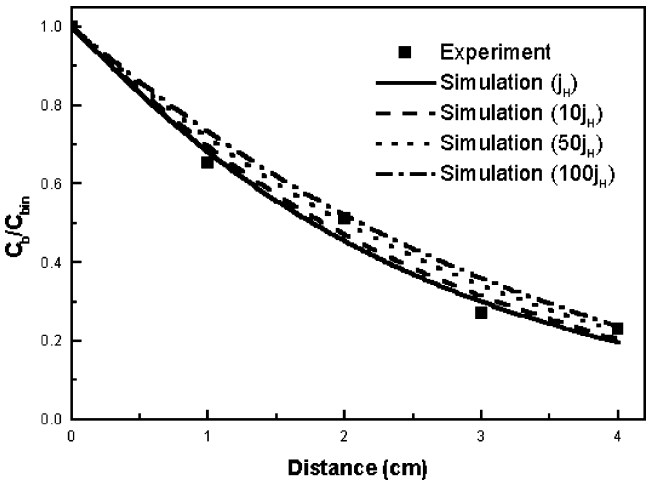

Figure 8. Sensitivity of the CT concentration profiles to changes in hydrogen generation current density. The current density calculated from Tafel's equation (eq 18) is increased by factors of 10, 50, and 100 in the model simulations used to generate the CT concentration profiles. For these results, the liquid superficial velocity is 0.034 cm/s, the solution conductivity is 2.3 S/m, and the applied cathode potential is −0.6 V.

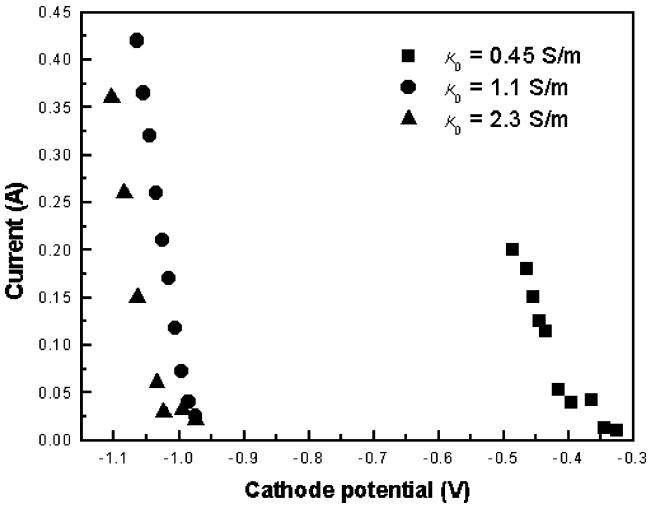

Figure 9. Measured total current at the downstream end of the cathode for the hydrogen generation reaction using solutions of various conductivities. The liquid superficial velocity is 0.04 cm/s.

artificially modified the value of j_H calculated from eq 18 by factors of 10, 50, and 100 (Figure 8). Results show that, under the conditions considered, CT removal is relatively insensitive to changes in the calculated current density for hydrogen generation: the overall CT removal fraction varied from 80.5% to 76.2% when j_H was changed by 2 orders of magnitude. These changes would clearly affect reactor performance in terms of power consumption, however.

Model Limitations. The model presented considers only processes that occur on the cathode. The boundary condition for the solution potential at the downstream end of the cathode was a zero-potential condition (eq 28); i.e., all solution potentials are referenced to a zero solution potential at the downstream end of the cathode. The same boundary condition has been applied to simulate the performance of porous electrodes in previous works.[21,22] Application of this condition implicitly assumes that there will be no charge-transport limitations between the end of the cathode and the anode. This is an adequate consideration when the solution conductivity is relatively high. For low solution conductivities (<1 S/m), however, the overall potential changes across the cathode and between the anode and cathode become important. Although the applied cathode potential is unchanged, the overpotential for the charge transfer reaction throughout much of the porous cathode is considerably lower in magnitude. Model predictions based on the stated boundary condition indicate that much of the cathode would be unreactive due to low overpotential. From measurements of the HER current in the absence of CT for various solution conductivities (Figure 9), it is evident that hydrogen evolution starts at much higher (less negative) cathode potentials in the lowest conductivity solution. This unexpected result leads us to speculate that the solution potential at the downstream end of the cathode is significantly larger than 0 V, leading to higher than expected overpotentials.

Current measurements in the CT-free experiments were supported by visual observations of hydrogen gas formation, primarily at the downstream end of the porous cathode. It is emphasized that model predictions of HER current were much lower than observations for

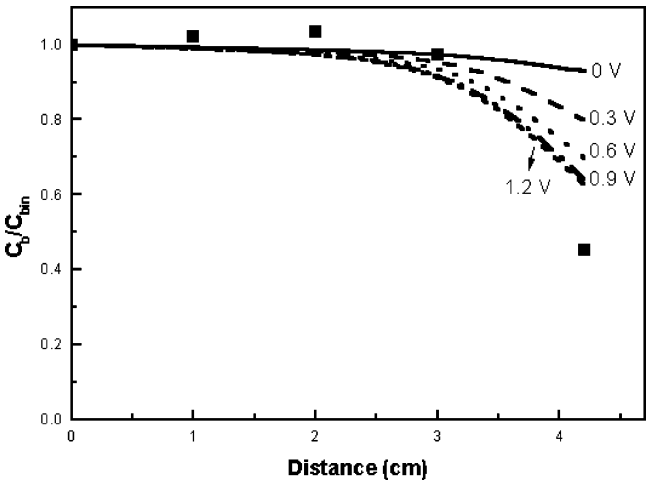

Figure 10. Experimental data and model predictions (solid line) for a low conductivity solution (0.067 S/m). The liquid superficial velocity is $3.16E^{-4}$ m/s. The applied cathode potential is 0.164 V. The boundary condition for solution potential at the downstream end of the cathode (0 V in the original model) was changed artificially. The figure shows the predictions for various assumed values for the boundary condition (in legend).

all low-conductivity simulations, and the observed effect of low conductivity on the relationship between HER current and cathode potential could not be anticipated within the current model framework. That is, in the 0.45 S/m conductivity experiment (Figure 9), the onset of measurable HER current was at $E_c = -0.32$ V. In the 1.1 and 2.3 S/m conductivity experiments, the onset of HER current was observed at a cathode potential of −0.97 V. It is hypothesized that, under low conductivity conditions, a significantly higher anode potential is needed to drive the anode reaction at the pace required to match the cathode reaction. Under those circumstances, the assumed zero-potential boundary condition at the downstream end of the cathode is violated.

Model predictions obtained by varying the downstream boundary conditions in low conductivity solutions are summarized in Figure 10. Both model and experiments indicated that the first three-fourths of the cathode was inactive. Observed degradation of CT occurred only in the last quarter of the cathode. However, the model predicted essentially no removal of CT when the zero-potential boundary condition was employed. Specifying a positive boundary solution potential improved the fit between model and experiment while maintaining the same spatial relationship for CT removal. The overall removal of CT increased monotonically up to $\phi_{s,L} = 0.9$ V. After that, removal predictions were essentially independent of the value selected for the boundary solution potential. At that point, the removal efficiency was controlled by mass transfer limitations because the rate constant for the charge-transfer reaction was more than 3 orders of magnitude higher than the mass transfer coefficient (calculation not shown). The highest predicted removal (38%) was significantly lower than the experimental value of 55%. The difference arose, at least in part, from CT stripping via H_2 gas evolution. At an observed HER current of 0.18 A, H_2 gas evolved at a rate of 2.7 mL/min (1 atm, 25 °C). Because the Henry's law constant for CT in water at 25 °C is 1.23,[24] and the liquid flow rate was 15 mL/min, stripping alone can account for removal of 22% of the total observed CT removal. The exercise is based on the assumption of instantaneous equilibrium between gas- and liquid-phase CT concentrations.

Conclusion

The electrochemical reduction of aqueous-phase CT in a continuous-flow reactor with a porous copper electrode is feasible. Removal of CT increases with lower (more negative) cathode potentials until hydrogen evolution becomes excessive. At that point, the increase in solution potential due to hydrogen generation offsets further change in cathode potential and limits further improvement in reactor performance. Carbon tetrachloride removal efficiency was predicted to vary inversely with the liquid velocity when the hydrodynamic residence time was held constant by shortening the reactor length. The explanation for this trend lies primarily in the distribution of solution potential within the porous cathode. At solution conductivities less than 1.0 S/m, both experiment and simulation showed that reactor performance is seriously handicapped by solution potential in the porous cathode. Model predictions of reactor performance were in reasonable agreement with experimental results for high conductivity solutions (≥1.0 S/m). At lower conductivities, calculations show that discrepancies between the model predictions and experimental results arise because the zero-potential boundary condition at the downstream end of the cathode becomes untrustworthy.

Literature Cited

(1) Vogel, T. M.; Criddle, C. S.; McCarty, P. L. Transformation of halogenated aliphatic compounds. *Environ. Sci. Technol.* **1987**, *21*, 722.

(2) Bouwer, E. J.; Wright, J. P. Transformations of trace halogenated aliphatics in anoxic biofilm columns. *J. Contam. Hydrol.* **1988**, *2*, 155.

(3) Assaf-anid, N.; Hayes, K. F.; Vogel, T. M. Reductive dechlorination of carbon tetrachloride by cobalamin(II) in the presence of dithiothreitol. *Environ. Sci. Technol.* **1994**, *28*, 246.

(4) Chiu, P. C.; Reinhard, M. Metallocoenzyme-mediated reductive transformation of carbon tetrachloride in titanium(III) citrate aqueous solution. *Environ. Sci. Technol.* **1995**, *29*, 595.

(5) Chiu, P. C.; Reinhard, M. Transformation of carbon tetrachloride by reduced vitamin B_{12} in aqueous cysteine solution. *Environ. Sci. Technol.* **1996**, *30*, 1882.

(6) Gillham, R. W.; O'Hannesin, S. F. Enhanced degradation of halogenated aliphatics by zerovalent iron. *Ground Water* **1994**, *32*, 958.

(7) Johnson, T. L.; Scherer, M. M.; Tratnyek, P. G. Kinetics of halogenated organic compound degradation by iron metal. *Environ. Sci. Technol.* **1996**, *30*, 2634.

(8) Matheson, L. J.; Trantnyek, P. G. Reductive dehalogenation of chlorinated methanes by iron metal. *Environ. Sci. Technol.* **1994**, *28*, 2045.

(9) Orth, S. W.; Gillham, R. W. Dechlorination of trichloroethene in aqueous solution using Fe(0). *Environ. Sci. Technol.* **1996**, *30*, 66.

(10) Liu, Z. J.; Arnold, R. G.; Betterton, E. A.; Festa, K. D. Electrolytic reduction of CCl_4 − effects of cathode material and potential on kinetics, selectivity, and product stoichiometry. *Environ. Eng. Sci.* **1999**, *16*, 1.

(11) Scherer, M. M.; Westall, J. C.; Ziomek-Moroz, M.; Tratnyek, P. G. Kinetics of carbon tetrachloride reduction at an oxide-free iron electrode. *Environ. Sci. Technol.* **1997**, *31*, 2385.

(12) Criddle, C. S.; McCarty, P. L. Electrolytic model system for reductive dehalogenation in aqueous environment. *Environ. Sci. Technol.* **1991**, *25*, 973.

(13) Cheng, I. F.; Fernando, Q.; Korte, N. Electrochemical dechlorination of 4-chlorophenol to phenol. *Environ. Sci. Technol.* **1997**, *31*, 1074.

(14) Li, T.; Farrell, J. Reductive dechlorination of trichloroethene and carbon tetrachloride using iron and palladized-iron cathodes. *Environ. Sci. Technol.* **2000**, *34*, 173.

(15) Lambert, F. L.; Hasslinger, B. L.; Franz, R. N. The total reduction of carbon tetrachloride at the glassy carbon electrode. *J. Electrochem. Soc.* **1975**, *122*, 737.

(16) Chen, G.; Betterton, E. A.; Arnold, R. G. Electrolytic oxidation of trichloroethylene using a ceramic anode. *J. Appl. Electrochem*. **1999**, *29*, 961.

(17) Nagaoka, T.; Yamashita, J.; Takase, M.; Ogura, K. Composite electrodes consisting of metal and oxidized carbon particles for complete degradation of trichlorethylene in acetonitrile. *J. Electrochem. Soc*. **1994**, *141*, 1522.

(18) Calmidi, V. V.; Mahajan, R. L. Forced convection in high porosity metal foams. *J. Heat Transfer* **2000**, *122*, 557.

(19) Lu, T. J.; Stone, H. A.; Ashby, M. F. Heat transfer in open-cell metal foams. *Acta Mater*. **1998**, *46*, 3619.

(20) Liu, Z. J.; Betteron, E. A.; Arnold, R. G. Electrolytic reduction of low molecular weight chlorinated aliphatic compounds: structural and thermodynamic effects on process kinetics. *Environ. Sci. Technol*. **2000**, *34*, 804.

(21) Pickett, D. J. *Electrochemical Reactor Design*; Elsevier Scientific Publishing Company: Amsterdam, The Netherlands, 1979.

(22) Doherty, T.; Sunderland, J. G.; Roberts, E. P. L.; Pickett, D. J. An improved model of potential and current distribution within a flow-through porous electrode. *Electrochim. Acta* **1996**, *41*, 519.

(23) Freeze, R. A.; Cherry, J. A. *Groundwater*; Prentice Hall Inc.: Englewood Cliffs, NJ, 1979.

(24) LaGrega, M. D.; Buckingham, P. L.; Evans, J. C. *Hazardous Waste Management*; McGraw-Hill: New York, 1994.

Received for review July 15, 2003
Revised manuscript received December 1, 2003
Accepted December 5, 2003

IE030591C